buildings

MDPI

Review

Non-Ferrous Metal Smelting Slags for Thermal Energy Storage: A Mini Review

Meichao Yin [1], Yaxuan Xiong [1,*], Aitonglu Zhang [1], Xiang Li [1], Yuting Wu [2], Cancan Zhang [2], Yanqi Zhao [3] and Yulong Ding [4]

[1] Beijing Key Lab of Heating, Gas Supply, Ventilating, and Air Conditioning Engineering, Beijing University of Civil Engineering and Architecture, Beijing 100044, China; 2108140423015@stu.bucea.edu.cn (M.Y.); 2108140422022@stu.bucea.edu.cn (A.Z.); 2108590022221@stu.bucea.edu.cn (X.L.)
[2] Beijing Key Laboratory of Heat Transfer and Energy Conversion, Beijing University of Technology, Beijing 100124, China; wuyuting@bjut.edu.cn (Y.W.); zcc@bjut.edu.cn (C.Z.)
[3] School of Energy Science and Engineering, Nanjing Tech University, Nanjing 211816, China; hazhaoyq@126.com
[4] Birmingham Center for Energy Storage, University of Birmingham, Birmingham B15 2TT, UK; y.ding@bham.ac.uk
* Correspondence: xiongyaxuan@bucea.edu.cn

Abstract

The metallurgical industry is integral to industrial development. As technology advances and industrial demand grows, the annual output of metallurgical waste slag continues to rise. Combined with the substantial historical stockpile, this has made the utilization of metallurgical slag a new research focus. This study comprehensively sums up the composition and fundamental characteristics of metallurgical waste slag. It delves into the application potential of non-ferrous metal smelting waste slag, such as copper slag, nickel slag, and lead slag, in both sensible and latent heat storage. In sensible heat storage, copper slag, with its low cost and high thermal stability, is suitable as a storage material. After appropriate treatment, it can be combined with other materials to produce composite phase change energy storage materials, thus expanding its role into latent heat storage. Nickel slag, currently mainly used in infrastructure materials, still needs in-depth research to confirm its suitability for sensible heat storage. Nevertheless, in latent heat storage, it has been utilized in making the support framework of composite phase change materials. While there are no current examples of lead slag being used in sensible heat storage, the low leaching concentration of lead and zinc in lead slag concrete under alkaline conditions offers new utilization ideas. Given the strong nucleation effect of iron and impurities in lead slag, it is expected to be used in the skeleton preparation of composite phase change materials. Besides the aforementioned waste slags, other industrial waste slags also show potential as sensible heat storage materials. This paper aims to evaluate the feasibility of non-ferrous metal waste slag as energy storage materials. It analyses the pros and cons of their practical applications, elaborates on relevant research progress, technical hurdles, and future directions, all with the goal of enhancing their effective use in heat storage.

Keywords: non-ferrous metal smelting slags; copper slag; nickel slag; lead slag; energy storage; sensible heat storage; latent heat storage

check for updates

Academic Editor: Andrea Petrella

Received: 9 June 2025
Revised: 1 July 2025
Accepted: 4 July 2025
Published: 7 July 2025

Citation: Yin, M.; Xiong, Y.; Zhang, A.; Li, X.; Wu, Y.; Zhang, C.; Zhao, Y.; Ding, Y. Non-Ferrous Metal Smelting Slags for Thermal Energy Storage: A Mini Review. *Buildings* **2025**, *15*, 2376. https://doi.org/10.3390/buildings15132376

Copyright: © 2025 by the authors. Licensee MDPI, Basel, Switzerland. This article is an open access article distributed under the terms and conditions of the Creative Commons Attribution (CC BY) license (https://creativecommons.org/licenses/by/4.0/).

1. Introduction

As society advances, energy demand exhibits a consistent upward trajectory. The development of efficient and clean energy sources has emerged as a pressing imperative

confronting nation globally. Notably, the supply and demand dynamics of various energy forms, such as solar energy, wind energy, industrial waste heat, compressed air waste heat, and off-peak electricity, exhibit distinct temporal and spatial disparities [1]. Energy storage technology serves as a viable solution to address this predicament, facilitating the decoupling of supply and demand within the energy system. Furthermore, it is noteworthy that over 90% of the primary energy consumed globally is in the form of thermal energy [2].

Thermal energy storage (TES) assumes a broad and pivotal role in the realm of efficient and sustainable energy utilization. By enabling the storage and strategic release of thermal energy, TES technologies contribute significantly to enhancing energy efficiency, mitigating energy supply–demand imbalances, and fostering the transition towards a more sustainable energy future [3]. In summary, thermal energy storage (TES) encompasses three primary modalities: sensible heat storage (SHS), latent heat storage (LHS), and thermochemical heat storage (TCHS) [4,5]. When compared to l LHS and thermochemical heat storage, SHS offers a simpler operational principle, is technically more likely to implement, exhibits lower costs, and demonstrates high safety standards. However, it is characterized by relatively low heat storage density and significant temperature variations. LHS primarily leverages materials to absorb or release substantial amounts of latent heat during phase transitions, offering high heat storage density, minimal temperature fluctuations, excellent chemical stability, and enhanced safety. Nonetheless, the heat transfer efficiency at the liquid–solid interface is poor, and certain water-based and salt-based phase change materials (PCMs) are susceptible to supercooling phenomena. Thermochemical thermal storage boasts high energy density, a broad operating temperature range, and minimal long-term storage heat loss. Nevertheless, it is technically intricate, necessitates a substantial one-time investment, and is prone to safety concerns, coupled with a relatively short cycle life. Developing efficient thermal energy storage systems (TESS) utilizing thermal energy storage materials (TESMs) presents a viable solution to the challenge of energy supply–demand mismatch and contributes to mitigating the depletion of fossil resources [6–10]. The advantages and disadvantages of different heat storage methods are shown in Figure 1. Thermal storage materials should ideally meet several criteria, including low cost, substantial storage capacity, high thermal capacity, non-toxicity, and compatibility with conventional heat transfer fluids and storage tank materials. Utilizing the vast quantities of slag waste generated by the metallurgical industry as thermal storage materials presents a promising avenue for addressing these requirements. This approach not only mitigates environmental pollution but also enhances the efficiency of resource utilization. Consequently, investigating the feasibility and effectiveness of employing metallurgical slag waste as a thermal storage material holds significant importance.

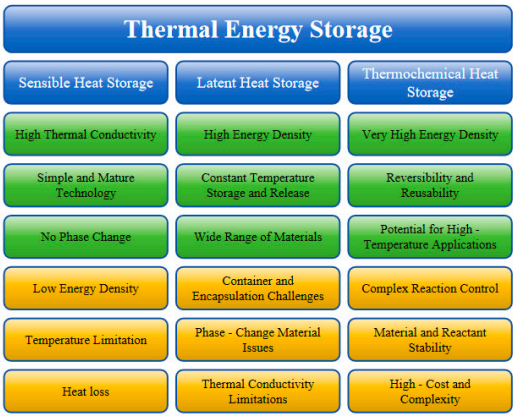


Figure 1. Advantages and disadvantages of different heat storage methods.

Metallurgical waste encompasses a diverse array of solid residues produced throughout the metallurgical industry's manufacturing processes. It primarily comprises blast furnace slag and steel slag (SS), which are byproducts of iron smelting operations. Additionally, it includes various non-ferrous metal slags generated from the smelting of metals such as copper, lead, zinc, and nickel. Furthermore, RM, a residue resulting from the extraction of alumina from bauxite, and minor quantities of iron oxide slag produced during the steel rolling process are also classified as metallurgical waste.

Slag indeed represents a multifaceted byproduct arising from the iron and steel manufacturing processes. During these procedures, flux materials are introduced into the molten iron or steel to facilitate the removal of impurities. The flux materials undergo chemical reactions with the impurities, effectively separating them from the molten metal and leading to the formation of slag. This slag, once cooled and solidified, can be further processed or utilized in various applications, including construction materials and road aggregates, thus contributing to resource efficiency and sustainability within the metallurgical industry [11]. For every ton of pure iron and steel manufactured, approximately 300 kg of blast furnace slag (BFS) and 100–200 kg of either basic oxygen furnace slag (BOFS) or electric arc furnace slag (EAFS) are generated as by-products [12]. It is projected that global crude SS production in 2024 will range between approximately 330 million and 390 million tons, while the output of metallurgically processed SS (following metal recovery) is anticipated to fall within the range of 190 million to 290 million tons. Accurate data on actual slag generation in the United States remain unavailable; however, based on 2024 slag sales statistics, it is estimated that the volume of slag traded or utilized in the US market is approximately 16 million tons [13]. In Europe, approximately 45 million metric tons of slag is generated annually as a byproduct of iron and steel production processes [14], By comparison, China generates over 120 million metric tons of SS annually, representing approximately half of the global annual SS output [15]. The applications of SS shows in Figure 2.



Figure 2. Applications of steel slag [15].

Copper slag is a byproduct of the copper production industry, specifically generated through pyrometallurgical copper smelting processes that utilize copper concentrate. This slag is abundant in valuable metals, including copper (Cu), cobalt (Co), nickel (Ni), and zinc (Zn) [16,17]. Approximately 2.2 to 3 tons of copper slag are generated per ton of copper produced. These wastes are predominantly managed and treated in proximity to the smelting facilities [18–20]. There is a substantial number of copper processing plants operating globally. A literature review conducted from 2005 to 2014 reveals that the annual slag production amounts to be approximately 24.6 million tons [21,22]. By 2021, It is estimated that the pyrometallurgical process will generate more than 40 million tons of copper slag annually [16,23]. As the largest producer of copper ore globally, Asia generates approximately 7.26 million tons of copper slag annually [24,25]. North America, Europe, South America, Africa, and Oceania generate approximately 59,000, 55,600, 41,800,

12,300, and 4500 tons of copper slag annually, respectively [26]. As industrial demand continues to surge, the annual production of copper slag is rising steadily. Relying solely on simple stacking for its disposal not only consumes extensive land resources but also entails potential safety risks and environmental pollution hazards [23,27–31]. The applications of copper slag are shown in Figure 3.

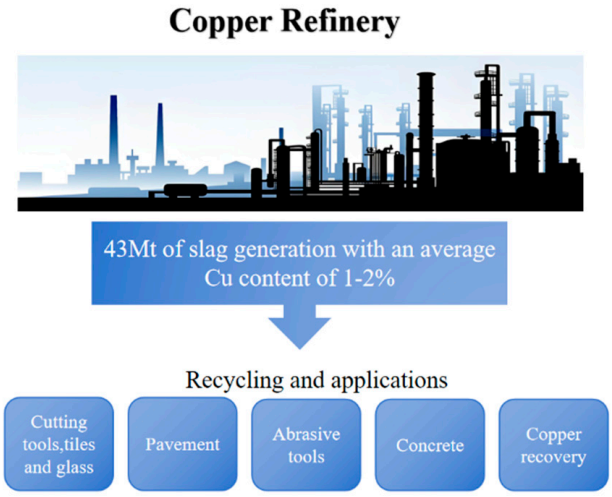


Figure 3. The applications of copper slag [32].

Ferronickel slag (FNS), commonly referred to as nickel slag, is a granulated solid waste residue generated through water quenching or natural cooling processes during the pyrometallurgical production of stainless steel products from laterite nickel ore or nickel sulfide ore [33,34]. With the ongoing expansion of the nickel smelting industry's scale, the volume of nickel slag is on the rise. Statistics indicate that for every 1 ton of nickel produced, 6–16 tons of nickel slag are discharged [34]. The survey indicates that global nickel slag emissions are projected to surpass 60 million tons, with China alone contributing over 30 million tons annually [35]. Nickel slag has emerged as the fourth-largest metallurgical waste, following high slag, SS, and RM [36]. Currently, the utilization rate of nickel slag is exceedingly low, and its primary disposal methods include stockpiling, deep-sea landfill, and underground filter-press backfilling. These approaches not only consume valuable land resources but also lead to severe pollution of soil and water quality [37,38].

With the rapid advancement of the iron and steel industry, as well as the lead and zinc and other non-ferrous metal smelting industries, two primary methods are employed for lead and zinc extraction: pyrometallurgy and hydrometallurgy. This paper primarily centers on the waste residue generated during the pyrometallurgical imperial smelting process (ISP). The precise composition of lead–zinc slag is intricately linked to both the raw materials utilized and the specific smelting process employed [39]. In the pyrometallurgical process, both shaft furnace slag and refining slag are generated. According to investigations, shaft furnace slag exhibits high mechanical strength and water solubility, rendering it primarily suitable for applications such as road construction, mining backfill, and as an insulation layer covering for waste dumps [39]. Per statistics from the China Nonferrous Metals Industry Association, the annual production of lead slag by Chinese lead smelting companies reached over 3 million tons in 2017, while the historical stockpile exceeded 100 million tons [40,41]. The disposal of lead slag primarily involves open stacking or simple landfilling, requiring an area exceeding 670 m^2 for every 10,000 tons of stacked lead slag [40,42], The waste slag produced during the lead–zinc refining process exhibits a highly complex composition. The presence of toxic heavy metals, including lead (Pb), zinc (Zn), and cadmium (Cd), in this slag poses substantial risks of soil contamination [42–44].

Thus, the effective management of lead slag through harmless treatment and resource utilization has emerged as a pressing issue that requires immediate attention to guarantee the long-term sustainability of the lead industry [45,46].

RM is a hazardous alkaline waste residue generated during the refining of alumina from bauxite. Typically, 1–1.5 tons of RM are produced for every ton of alumina extracted [47]. RM is an industrial waste residue rich in iron, containing approximately 42% iron oxide (Fe_2O_3) by mass [48], it contains a substantial amount of iron oxide (Fe_2O_3), which imparts its characteristic red hue. The increasing accumulation of RM presents substantial environmental risks, primarily due to its alkalinity, heavy metal content, and the extensive landfill space it requires [49]. According to literature reviews, the global annual production of RM is estimated to reach approximately 150 million metric ton [50]. The primary components of RM include SiO_2, Al_2O_3, CaO, and Fe_2O_3, which are insoluble residues formed during the Bayer process for alumina production [51,52]. RM is characterized by high water content and the presence of alkali, heavy metals, and other harmful components. Its pH value can exceed 11, rendering it highly alkaline and posing a significant threat to environmental and ecological systems [53–55]. The high soluble alkalinity of RM significantly impedes its sintering into viable building materials, representing the primary obstacle to its large-scale recycling in the construction industry [56]. In addition, RM stored in dams or dikes requires regular maintenance, resulting in an additional cost of USD 7–15 per ton, which indirectly raises aluminum production costs by up to 5% [57]. The hazards posed by RM are multifaceted, encompassing land occupation, soil contamination, air pollution, structural erosion of buildings, and groundwater pollution. Consequently, the treatment and utilization of RM warrant heightened attention, and more scientific and effective approaches must be adopted to mitigate its environmental hazards. In a mini review on sewage sludge and red mud recycling for thermal energy storage, Zhang et al. [5] described in detail the properties of RM and its application in the field of heat storage.

It is estimated that metal smelting contributes over 40% of anthropogenic heavy metal emissions, resulting in the pollution of approximately 1.5 million hectares of land globally [58]. By 2019, China's industrial waste generation had reached 35.43 billion tons, with the majority comprising blast furnace slag, SS, fly ash (FA), RM, coal gangue and desulfurization gypsum [59]. At present, the predominant methods for managing industrial waste in China are stockpiling and landfilling. These approaches consume substantial land resources and pose a significant risk of heavy metal leaching, thereby threatening local ecosystems [60,61]. Slag waste management in China faces significant challenges. The current disposal methods for slag waste predominantly rely on traditional stacking and landfilling. However, the complexity and economic inefficiency of metal recovery technologies hinder their widespread adoption. Consequently, utilizing slag waste as a heat storage material represents a promising alternative. Nevertheless, several technical challenges must be addressed to enable its broad application in this direction. Specifically, it is essential to investigate the composition, structure, and properties of slag waste and develop optimal utilization and modification strategies for its use as a heat storage material. Additionally, the design and optimization of heat storage systems must be considered to enhance energy efficiency and ensure system safety. Innovative research and development efforts are essential to fully unlock the potential of slag waste in sustainable energy applications.

Solid and liquid materials are both employed for sensible heat storage. Solid materials involve sand [62], rock [63], pebbles [64], concrete [65], and gravel [66], while liquid ones cover water [67], oil [68], glycerol [69], and molten salt [70]. Prabhat [71] demonstrated that waste motor oil can be used as an alternative to Servotherm as a sensible heat storage medium in solar air heaters. This study focuses on solid-state storage materials, Abddaim

et al. [72] assessed rhyolite, andesite, diorite, and granodiorite, deeming them promising for high-temperature heat storage. Grirate et al. [73] examined six Moroccan rocks—quartzite, basalt, granite, slate, cipolin, and marble—singling out basalt for its superior thermal properties, especially heat capacity and performance in thermally stratified storage. Liu et al. [74] found basaltic glass exhibits heightened specific heat capacity, overall heat capacity, and thermal conductivity. Between 100 and 1000 °C, its average heat capacity is 3.164 MJ/(kg·K), allowing BG-1 to store up to 2847.6 MJ/m^3. Its thermal conductivity fluctuates between 1.19 and 1.60 W/(m·K) during 200–1000 °C thermal cycling. Overall, this basalt-based glass offers benefits like low cost, environmental suitability, enhanced thermal capacity, higher conductivity, and stability across broad temperatures, compared to other sensible heat storage media. Santos et al. [75] put forward hematite as a viable heat-absorbing material via numerical modeling and inversion. Khare et al. [76] found that alumina, silicon carbide, high-temperature concrete, graphite, cast iron, and steel are suitable for latent heat storage between 500 and 750 °C. These results show that natural materials like rocks, concrete, ceramics, and glass have potential in sensible heat storage. Ideal sensible heat storage materials should have high specific heat capacity, good thermal conductivity, mechanical durability, affordability, and wide availability [77]. Rocks and concrete provide benefits like low cost and high heat capacity, but their thermal conductivity is lower than metals, which are often more expensive. Steel slag has a high specific heat capacity (up to 0.95 J/(g·K)), good thermal conductivity, and favorable friction. Zhang et al. [78] used high-temperature-treated steel slag to develop efficient heat storage materials. This paper focuses on non-ferrous metallurgical byproducts. It aims to summarize current research and inspire new sensible heat storage solutions.

Latent heat storage uses PCMs to absorb and release energy. Common PCMs include inorganic salts, hydrated salts, and organic compounds. To prevent leakage, they are typically encapsulated in porous skeletons. Common skeleton materials include SiO_2 [79,80], $Mg(OH)_2$ [81], $Ca(OH)_2$ [82], Al_2O_3 [83] diatomite [84], expanded vermiculite [85,86], attapulgite [87], metal foam [88], expanded perlite [89], and expanded graphite [90], and so on. PCMs are divided into organic and inorganic categories, both applicable across a wide temperature range. Ruilong Wen et al. [91] made a series of pretreated attapulgite-based composite PCMs by thermal and acid activation with various fatty acids. Soleimanpour et al. [92] used a sintering process to make $NaNO_3$/diatomite PCC, adding nano-expanded graphite and nano-diamond particles to boost thermal conductivity for high-temperature use. Rathore [93] integrated expanded graphite and expanded vermiculite via vacuum impregnation with PCM to produce PCC. Adding expanded graphite raised thermal conductivity by 114.4% and ensured stable thermal performance over 1000 heating and cooling cycles. Using natural skeleton materials can be expensive and lead to high carbon emissions due to the demands of resource extraction and processing. Consequently, many researchers are now exploring solid waste materials as alternative sources for skeleton structures. Fan et al. [94] utilized semi-coke ash, a solid waste product, as a supporting matrix and sodium carbonate as the PCM to create shape-stable phase change composites. The optimal sample achieved a heat storage density of 961.58 J/g and a maximum thermal conductivity of 1.306 W/(m·K), indicating strong commercial potential. Yang et al. [95] developed shape-stable phase change composites using SS and carbide slag (CS) as supporting matrices and $NaNO_3$ as the PCM. Their analysis revealed that the samples retained excellent performance even after 1307 thermal cycles, suggesting promising application prospects. Researchers are increasingly exploring industrial byproducts as skeleton materials for composite phase change heat storage systems.

In summary, the treatment and utilization of slag waste present a complex and urgent challenge. This study systematically reviews the composition and fundamental properties

of metallurgical industry slag waste, with a particular emphasis on the potential applications of various industrial slags—such as copper slag, nickel slag, and lead slag–in both SHS and LHS systems. By analyzing the thermophysical characteristics and phase change behaviors of these slags, the study aims to elucidate their viability as sustainable heat storage materials, thereby contributing to the advancement of circular economy principles in industrial waste management

2. Materials and Methods

2.1. Copper Slag

The primary constituents of copper slag typically include iron silicate compounds, magnetite (Fe_3O_4), iron oxides (such as Fe_2O_3 and FeO), and trace metals [96–98]. The copper slag exhibits an irregular morphology (as illustrated in Figure 4), with its density primarily influenced by the iron content [99]. As demonstrated in Table 1, copper slag and SS exhibit comparable physical properties. The sample numbers listed in Table 1 are sourced from prior references. This study primarily investigates the application of copper slag.



Figure 4. Copper slag sample [99].

Table 1. Thermophysical properties of various slags obtained from the present study and the literature.

Slag Type	Sample ID	Density ρ [kg/m^3]	Thermal Conductivity K [W/(m·k)]	Specific Heat Capacity Cp [J/(g·k)]	Thermal Stability [°C]	Reference
Copper slag	ES-N [a,b]	3500	1.595	0.7–1.1	up to800	[99]
Copper slag	ES-A [a]	3700	2.173	1.4–1.5	up to 800	[99]
Copper slag	Curto C. Slag	4350	-	0.670–1.004	up to 1200	-
Copper slag	Slag P [a]	3600	0.8	0.571–1.180	up to 800	[100]
Copper slag	Slag B	3700	1.1	0.650–0.990	up to 800	[100]
Steel slag	EAF 1 [a]	3430	1.47	0.865	up to 1000	[101]
Steel slag	EAF 2	4110	1.51	0.837	up to 1000	[101]
Steel slag	Slag 1	3430	1.65–1.23	0.710–0.950	up to 1100	[102]
Steel slag	Slag 2	3770	1.50–1.73	0.690–0.890	up to 1100	[102]
Steel slag	S slag	3600	1.695–1.74	0.713–0.858	up to 1000	[77]
Steel slag	C slag	3700	1.84–1.75	0.717–0.975	up to 1000	[77]

[a] Value for parametric analysis. [b] Thermal stability of the sample.

2.2. Nickel Slag

Nickel slag is typically obtained in blocks of varying sizes [103]. Due to variations in ore type and smelting processes employed, the composition of nickel slag exhibits slight

differences. However, its primary constituents remain SiO_2, Fe_2O_3 and MgO The mass fractions of these components typically range as follows: SiO_2 (25–50%), Fe_2O_3 (25–45%), and MgO (1–30%) [33–38,103–106]. The composition of furnace nickel slag is affected by ore type, smelting process, and cooling method. Presently, air cooling and water quenching are the two main cooling methods employed. Air cooling involves directly discharging the slag outdoors to allow natural solidification. Quenching involves immersing the slag in water to induce rapid cooling and solidification. The chemical composition of FNS is highly diverse and is primarily influenced by these factors. In Table 2, air cooling is A and quenching is W. In recent decades, driven by the rapid expansion of the metallurgical industry, China has emerged as the world's largest consumer of nickel resources. By 2022, China accounted for 36% of global nickel production. However, this growth has triggered a cascade of environmental and resource management challenges. Specifically, the utilization rate of nickel slag (a byproduct of nickel smelting) remains alarmingly low, at 8–10%, despite its potential as a secondary resource.

Consequently, vast quantities of nickel slag accumulate on the surface year-round, posing significant threats to soil quality, ecosystem health, and long-term environmental sustainability. This issue underscores the urgent need for innovative strategies to enhance the resource recovery and valorization of nickel slag [107].

According to the generation mechanisms and classifications of different smelting processes, FNS can be divided into electric-furnace nickel slag (EFNS) and blast-furnace ferronickel slag (BFNS).

In the electric-furnace process, the mined nickel sulfide ore is initially calcined in a rotary kiln at temperatures between 750 and 800 °C, followed by crushing, grinding, and drying. Then, the processed ore is transferred to an electric furnace, where it is smelted at temperatures ranging from 1500 to 1600 °C. Finally, nickel is extracted through chemical extraction methods, and the molten slag is discharged. After cooling, EFN is formed [108], as shown in Figure 5.

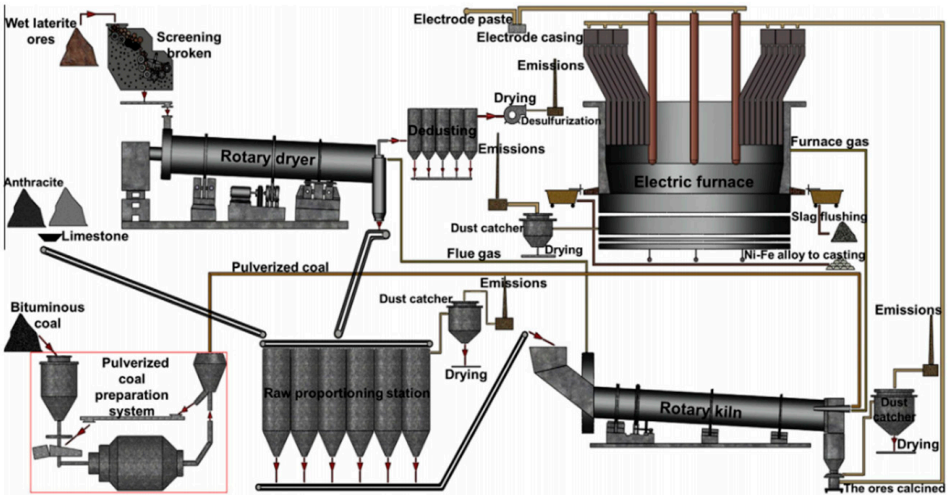


Figure 5. Schematic of the RKEF process with rotary dryer, rotary kiln and electric furnace [108].

Table 2. The chemical composition of FNS.

Samples	SiO_2	Al_2O_3	Fe_2O_3	CaO	MgO	K_2O	SO_3	Sum	Reference
EFNS-W	58.10	2.29	11.10	0.29	26.50	0.06	0.04	98.38	[109]
EFNS-A	62.80	1.95	7.13	2.07	24.70	0.02	0.03	98.7	[109]

Table 2. *Cont.*

Samples	SiO_2	Al_2O_3	Fe_2O_3	CaO	MgO	K_2O	SO_3	Sum	Reference
EFNS-W	46.10	4.46	12.25	6.75	27.12	0.07	0.14	96.89	[110]
EFNS-W	45.23	5.91	9.74	8.93	24.17	-	-	93.98	[111]
EFNS-W	32.74	8.32	43.83	3.73	2.76	-	-	91.38	[112]
EFNS-W	42.96	12.09	12.52	4.88	26.52	0.11	-	99.08	[113]
BFNS-W	27.31	21.82	1.57	32.72	8.64	-	-	92.06	[114]
BFNS-W	29.95	26.31	1.55	25.19	8.93	0.4	0.9	93.23	[110]
BFNS-W	31.76	14.84	0.6	36.44	9.08	-	0.04	92.76	[115]
BFNS-A	41.14	5.69	6.87	25.96	15.40	0.54	1.29	96.89	[116]

2.3. Lead Slag

Lead slag primarily consists of elements such as Ca, Fe, and Si. The slag particles are jet-black in color and have a particle size ranging from 2 to 20 mm [117]. Taking several old cassiterite polymetallic sulfide deposits in Yunnan as examples, after years of production, the local smelting operations have generated approximately 30 million tons (3000×10^4 t) of lead slag. Among this, 2.6 million tons (260×10^4 t) have been identified as hazardous waste, occupying an area of 920,000 square meters (92×10^4 m^2). Locally, lead ingots are produced through the sintering–roasting blast-furnace smelting process. The lead slag generated by this process is a high-temperature melt of high chemical complexity. It is composed of substances such as Fe_2O_3, SiO_2, Al_2O_3, CaO, MgO, and ZnO, and exists in the form of a mixture of compounds, solids, and co-products [118,119]. Lead–zinc slag contains a variety of oxides and rare metal elements. The contents of various compounds and metal elements in zinc–lead metallurgical slag are related to the ore-producing areas and smelting methods. Through literature research, as demonstrated in Table 3 it is found that the content of Fe_2O_3 is approximately 2.07–32.47%, that of FeO is 9.49–28.90%, $SiO_2$is 14.68–43.09%, CaO is 3.05–23.11%, Al_2O_3 is 1.73–6.22%, MgO is 0.15–5.44%, PbO is 1.12–12.28%, ZnO is 2.82–11.11%, and S is 0.2–9.0%.

Table 3. The chemical composition of the primary lead slag.

Fe_2O_3	FeO	CaO	SiO_2	Al_2O_3	MgO	ZnO	PbO	CuO	S	Reference
2.07	22.91	20.5	34.92	2.07	2.36	3.63	1.12	0.10	1.11	[120]
10.38	23.32	22.10	24.33	2.46	2.71	11.11	3.63	-	0.39	[121]
-	14.99	23.05	43.09	6.22	1.58	4.01	-	-	-	[122]
32.47	9.49	4.5	14.68	4.7	1.43	2.82	10.34	2.75	6.51	[123]
28.81	17.56	11.53	35.5	3.85	4.65	6.02	4.03	0.79	0.24	[123]
7.63	20.47	23.11	21.39	3.56	5.44	9.47	4.06	-	0.37	[119]
28.10	-	23.11	21.39	3.56	5.44	9.47	4.06	-	0.37	[124]
3.36	28.90	18.34	31.34	4.26	1.72	8.20	2.69	-	1.19	[125]
8.11	23.27	22.14	24.88	2.46	2.71	10.77	3.74	-	-	[126]
31.57	-	3.05	21.56	1.73	0.15	6.18	12.28	1.64	8.01	[127]

3. Application of Sensible Heat Storage

3.1. The Application of Copper Slag in Sensible Heat Storage

In 1984, Curto [128] put forward a preliminary proposal to use copper slag as a filling material for packed-bed thermal energy storage, highlighting its thermal, chemical, and mechanical stability up to 1000 °C. It is reported that the specific heat capacity of copper slag is approximately 1.188 J/(g K). In addition, Sibarani et al. [129] analyzed the specific heat capacity of the material in the temperature range from 300 °C to 900 °C, and the recorded values were between 0.93 J/(g·K) and 1.17 J/(g·K). Moreover, Calderón-Vásquez

et al. [99] analyzed the apparent oxygen content of Chilean copper slag samples. The results indicated that the values were between 0.8 J/(g·K) and 2.1 J/(g·K) in the temperature range from room temperature to 500 °C. However, it is worth noting that these *cp* results were not incorporated into the reference material to correct the measured *cp* values, which may lead to an overestimation of these values.

Ignacio et al. [99] revealed through software modeling and experiments that copper slag demonstrates a higher heat capacity (1.4–1.5 J/(g K)) compared to other materials. They assessed its potential as a heat storage material in a packed-bed system. Results showed that copper slag's high heat capacity helps form a steeper thermocline, enabling the maintenance of a lower heat storage loss rate. Moreover, with the same heat storage size, the energy density of copper slag is 138 kWh/m^3, while that of other byproducts is 129 kWh/m^3. A preliminary evaluation suggests that the application of copper slag as a filler in a packed-bed system is promising.

However, the tests by Ignacio Calderón Vásquez et al. are limited by the equipment's allowable temperature range, with a maximum of only 500 °C. This temperature positions copper slag as a competitor for molten-salt applications and a potential filler for molten-salt tanks. To determine the temperature limit for using copper slag, new high-temperature tests are needed, and its full potential as a storage material requires further study.

Navarro et al. [100,130] measured and compared the LHS properties of Al, Mg, Si, and Zn, along with those of the alloys 88Al–12Si and 60Al–34Mg–6Zn. Additionally, they further investigated the potential of utilizing copper slag as a low-cost SHS material in the heat storage system.

Ortega-Fernandez et al. [102] concluded that the SS produced by the EAF process is thermally stable below 1100 °C. Additionally, as the temperature of the slag increases, the structure of the slag will affect its thermal performance. Specifically, the higher the crystallinity, the lower the specific heat and the greater the thermal conductivity.

3.2. The Application of Nickel Slag in Sensible Heat Storage

Since the early 1980s, numerous scholars at home and abroad have dedicated themselves to the resource utilization of nickel slag. After decades of exploration and development, nickel slag resource utilization technologies have become relatively mature, primarily encompassing the extraction and recovery of valuable metals, its application as an auxiliary material in glass–ceramics, its use as a mixed material in cement production, the ecological utilization of nickel slag, and its employment as concrete aggregate in alloy production, wool production, mine landfilling, etc., as well as the preparation of new wall materials from nickel slag, such as thermal insulation blocks and unburned bricks.

Solid-waste-derived wall materials not only exhibit characteristics of high strength, energy conservation, and environmental protection but also effectively reduce production costs and resource waste. Given the high magnesium content in nickel slag, this characteristic can be fully leveraged to prepare high-quality wall refractory and thermal insulation materials.

Zhang et al. [131] examined the physical properties and microstructure of geopolymer slurry incorporating nickel slag/metakaolin and discussed the influence of nickel slag content on these characteristics. Their findings show that using 40% nickel slag not only enhances the compressive strength but also induces volume expansion behavior in the hardened slurry. This study represents a significant step toward developing alternative "low-carbon" adhesives using nickel slag as a raw material for the construction industry.

3.3. The Application of Lead Slag in Sensible Heat Storage

Buzatu et al. [132] indicated that lead slag exhibits uniform particle size, excellent shear resistance, and superior drainage performance, making it suitable as a base material for road waterproof coatings. However, using smelted lead slag as a subgrade material in natural conditions risks heavy metal leaching [133]. Owing its high iron content, lead slag can be utilized as an alternative to iron ore in cement clinker production. During clinker calcination, lead slag lowers the melting temperature, accelerates the reaction between $2CaO{\cdot}SiO_2$ and CaO to form $3CaO{\cdot}SiO_2$, and reduces free calcium oxide content [134]. Alwaeli et al. [135] explored the substitution of quartz sand with lead slag in concrete production and discovered that concrete incorporating lead slag demonstrated superior compressive strength compared to conventional concrete. Atzeni et al. [136] examined the leaching behavior of lead slag-based concrete under acidic and alkaline conditions. They found that at pH 5, the leaching concentrations of lead and zinc were detected at 228 mg/L and 30 mg/L, respectively, while in an alkaline environment, the maximum leaching concentrations of lead and zinc were 115 mg/L and 1.2 mg/L, respectively. Ceramic and glass technologies can serve as effective methods for hazardous waste treatment by immobilizing regulated heavy metals within a stable matrix [137]. If the composition of glass-forming agents (SiO_2, Al_2O_3, CaO) meets the requirements for vitrification, non-ferrous metal smelting slags can be a potential raw material for glass production [138].

3.4. Analysis and Comparisons for Sensible Heat Storage

Non-ferrous metal smelting slags, such as copper, nickel, and zinc slags, can be recycled and used as resources. Here are some details about these slags:

(1) Copper Slag: It is favored for its low cost and high thermal performance. This makes it a popular choice for developing sensible heat storage materials. Researchers have more experience in this area and it has been widely used in relevant applications.
(2) Nickel Slag: Rich in SiO_2, Al_2O_3, Fe_2O_3, and MgO, nickel slag has good cementing and durability. It is commonly used in building materials like concrete and road base materials. However, its thermophysical properties for SHS need more research.
(3) Lead Slag: Containing heavy metals like lead and cadmium, lead slag is under-researched in SHS. Its potential applications are hindered. Researchers are particularly interested in its behavior in alkaline conditions. It is found that proper alkaline conditions can significantly reduce heavy metal leaching. This paves the way for its potential uses in other fields.

4. Application of Latent Heat Storage

4.1. The Application of Copper Slag in Latent Heat Storage

Hao et al. [139] stated that copper slag, a major solid waste in the copper smelting industry, possesses significant economic and environmental value and requires clean utilization. Traditional recovery technologies are characterized by extended treatment durations, limited efficiency, and substantial energy demands. The authors proposed a short-term depletion method using stirring-enhanced hot copper slag as raw material. By leveraging the slag's latent heat, 90.13% of the copper can be recovered within 45 min, with the copper content in the tailings dropping to 0.23 wt%. Compared to industrial flotation, it can save $\geq$1250 MJ of energy per ton of copper slag and cut CO_2 emissions by 156 kg. Using hot copper slag as raw material fully uses the slag's latent heat, achieves targeted enrichment and recovery of copper and iron, and reduces copper slag generation at the source.

Ye et al. [140] fabricated core–shell structured macro-capsules by partially substituting bauxite in the shell with copper slag. These copper-slag-doped macro-capsules exhib-

ited remarkable thermal cyclic stability and durability, withstanding intensive melting-solidification cycle tests up to 500 times. The incorporation of copper slag into the shell of high-temperature PCMs can effectively enhance their SHS capacity, thermal conductivity, and thermal diffusivity. This study offers a novel method for the resource utilization of solid waste.

Using commercial solid aluminum balls (CSABs) as the core and copper slag and bauxite as raw materials, a double-layer ceramic shell was prepared, process is illustrated in Figure 6. The inner shell, made from alumina mullite ceramics synthesized with bauxite powder, is resistant to molten metal corrosion. Copper slag partially replaced bauxite to prepare ceramics with alumina, mullite, and Fe_2O_3 as the outer shell components.

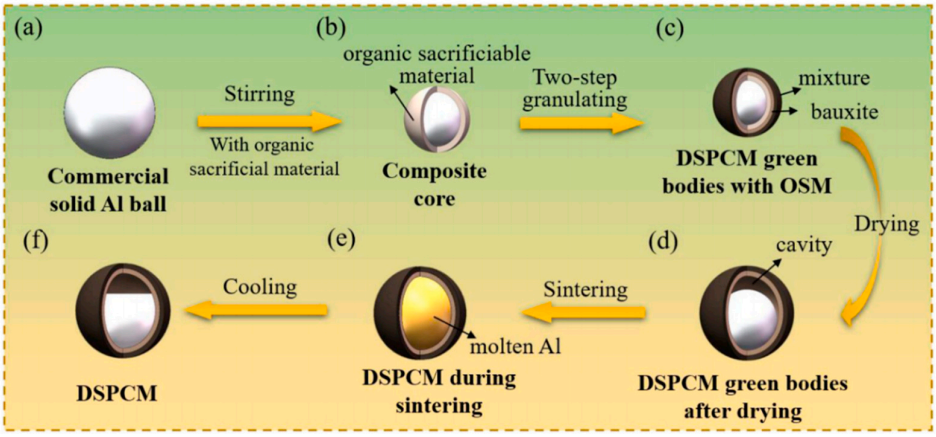


Figure 6. Preparation process of double shell high-temperature phase change material capsules [140].

Based on the open capsule depicted in Figure 7a, the double shell structure's integrity in all DSPCMs sintered at 1100 °C is confirmed. From the cross-sectional optical images and partially enlarged details of DSPCMs under the 3D microscope dark-field mode (Figure 7a), it is evident that DFT0 exhibits a single-layer shell, while DFT1, DFT2, and DFT3 form a double-layer shell after in situ sintering at 1100 °C. The single-layer shell is about 3 mm thick, with each layer of the double-shell structure being approximately 1.5 mm thick. A distinct boundary exists between the inner shell and the core, indicating that the inner shell possesses excellent corrosion resistance against the alloy, while the outer shell can prevent alloy leakage.

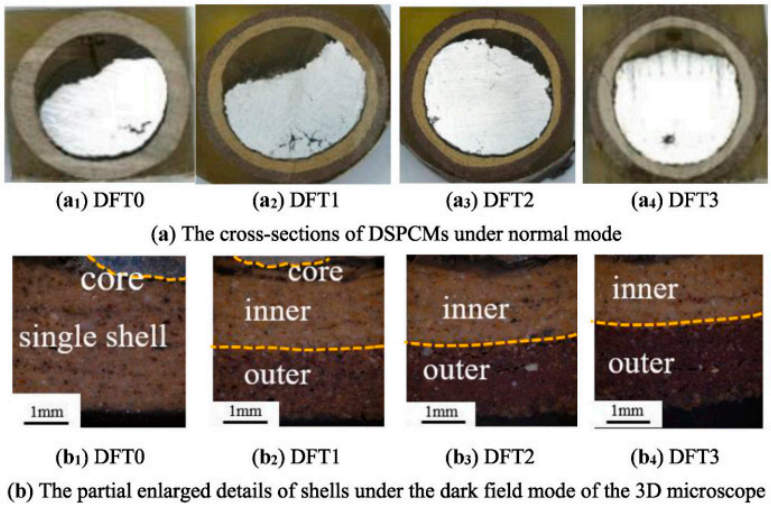


Figure 7. Optical image of DSPCM after sintering at 1100 °C [140].

The phase composition and microstructure of the double-layer ceramic shell were analyzed and characterized. As shown in Figure 8, thermal properties such as heat storage density, thermal conductivity, and durability were evaluated. This study offers a viable and promising technology for utilizing copper slag functionally and provides an effective solution for encapsulating high-temperature PCMs.

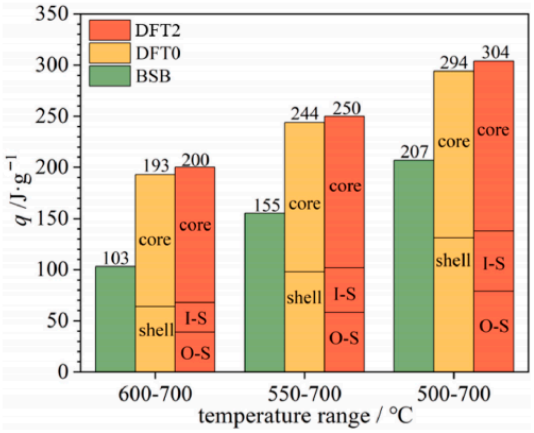


Figure 8. Comparison of thermal storage capacity of different macroscopic capsules in different temperature ranges [140].

Reference [140] investigated the use of copper slag in high-temperature PCM encapsulation. Based on bauxite and copper slag as raw materials, commercial solid aluminum spheres (CSABs) were successfully macro-encapsulated within ceramic shells in situ via a two-step granulation method. The organic material was discharged, creating a cavity between the core and the inner shell. This cavity accommodates the volume expansion of CSABs during melting. Through in situ sintering at 1100 °C, dense inner and porous outer ceramic shells were formed. This unique double-layer ceramic shell enables the macro-capsules to resist CSAB corrosion and prevent air inflow. Consequently, the addition of copper slag to the shell material does not compromise the durability of DSPCMs (double-shell phase change macro-capsules) after thermal cycle testing. After undergoing 500 thermal cycles ranging from 450 °C to 800 °C, DSPCMs with 20 wt% copper slag in the outer shell remained intact, with a mass increase of only 3.45%. Incorporating copper slag into DSPCMs promotes the formation of Fe_2O_3 in the outer shell, enhancing SHS capacity and thermal conductivity while improving heat transfer efficiency. The results demonstrate that copper slag holds significant potential for high-temperature heat storage systems. Using copper slag to make the skeleton material of phase change composite heat storage materials improved copper slag's resource utilization efficiency and saves natural resources.

4.2. The Application of Nickel Slag in Latent Heat Storage

Liu et al. [141] prepared cordierite–mullite porous ceramics (CMC) using secondary aluminum dross (SAD) and FNS as raw materials. These ceramics serve as the support framework for inorganic salts. $NaNO_3$/cordierite-mullite composite thermal storage materials were fabricated via a natural infiltration method and assessed their thermal storage performance through thermodynamic analysis. The framework material has a porous microstructure and a compressive strength over 30 MPa. The latent heats of the composites with varying FNS proportions were 76.4 J/g, 76.7 J/g, and 73.6 J/g, respectively. Reliability was verified through 100 thermal cycle experiments. When the temperature reaches 350 °C, the thermal conductance of all $NaNO_3$//porous ceramic composites exceeds 1.8 W/(m·K).

After thermal cycle testing, the composites' compressive strength experienced a slight reduction but still remained above 100 MPa, indicating their promising application potential.

In the experiment, secondary aluminum dross (SAD) and FNS were the main raw materials, and anthracite powder (<48 μm, 18 wt% ash content) was used as the pore-forming agent to increase the porosity of CMC. The $NaNO_3$/CMC composite preparation process includes ball milling, briquetting, calcination, and infiltration. Raw materials were processed via ball milling and mixing based on a pre-designed weight ratio [106]. The cordierite phase content in CMC increased with FNS addition. After briquetting and roasting, CMC with excellent mechanical strength and high porosity was obtained. $NaNO_3$/CMC composites were fabricated via a self-melting infiltration method: excess $NaNO_3$was placed in a porcelain boat with CMC and transferred to a 350 °C muffle furnace for 2 h to ensure complete melting of $NaNO_3$. Driven by capillary force, molten $NaNO_3$ spontaneously penetrated the pores of CMC and was confined within the pores upon cooling to room temperature. The composite preparation process is illustrated in Figure 9.

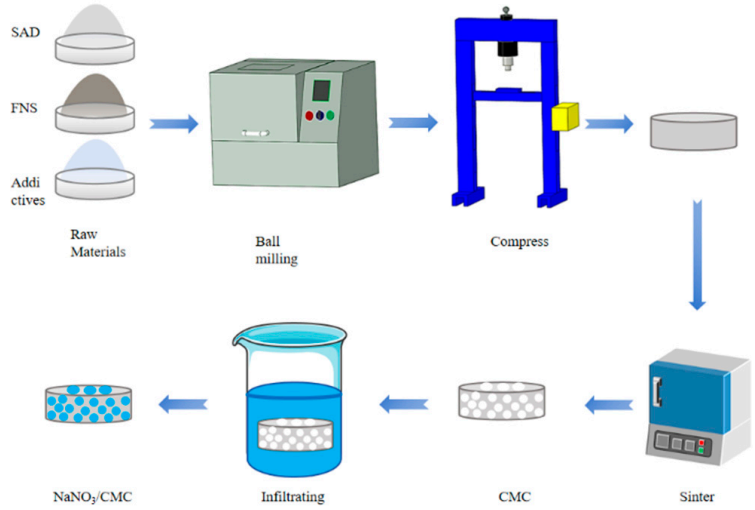


Figure 9. Preparation process of $NaNO_3$/porous ceramic composite material [141].

Samples were named based on the FNS content. For instance, CMC5 indicates 5 wt% FNS. XRD, DSC scanning, and thermal cycle tests revealed good chemical compatibility between $NaNO_3$ and the skeleton material. Through comparison of 30 groups of samples with different proportions, CMC5, CMC15, and CMC30—sintered at 1300 °C, 1250 °C, and 1250 °C, respectively—exhibited higher compressive strength of over 30 MPa and porosity of over 52%, making them selected as support skeletons. CMC as a support framework greatly boosts $NaNO_3$'s thermal conductivity, outperforming most solid waste-based C-PCMs made by mixing–sintering. Importantly, after 100 thermal cycles at 25 °C, $NaNO_3$/CMC composites keep a thermal conductivity over 1.8 W/(m·K). Owing to their high latent heat and thermal conductivity, $NaNO_3$/CMC30 composites are promising in low-cost medium-to-high-temperature heat storage and use areas like industrial waste heat recovery, renewable energy systems, and conventional power plant LHS systems.

From the XRD spectrum, it can be observed that the composite material obtained in this experiment exhibits good chemical compatibility. Meanwhile, the SEM image and EDS analysis of the $NaNO_3$/CMC composite were conducted, revealing that molten $NaNO_3$ fully fills the CMC support's pores, creating a dense structure.

From Figure 10 the DSC curves of the $NaNO_3$/CMC composite during heating and cooling indicates that the $NaNO_3$/CMC composite exhibits thermal behavior similar to that of pure $NaNO_3$, with a reversible solid–liquid phase transition occurring at approximately 300 °C. The melting latent heats of $NaNO_3$/CMC5, $NaNO_3$/CMC15, and $NaNO_3$/CMC30

were 76.4 J/g, 76.7 J/g, and 73.6 J/g, respectively, accounting for 43.5%, 43.6%, and 41.9% of that of pure $NaNO_3$. The initial melting temperature of pure $NaNO_3$ (305.7 °C) was higher than those of the $NaNO_3$/CMC composites ($NaNO_3$/CMC5: 305.1 °C; $NaNO_3$/CMC15: 305.2 °C; $NaNO_3$/CMC30: 304.8 °C). It was observed that the melting temperature increased with the increase in $NaNO_3$ content, which may be attributed to the high vapor pressure within the CMC pores [142]. The $NaNO_3$/CMC composites prepared in this study possess latent heats comparable to or even higher than those of similar materials.

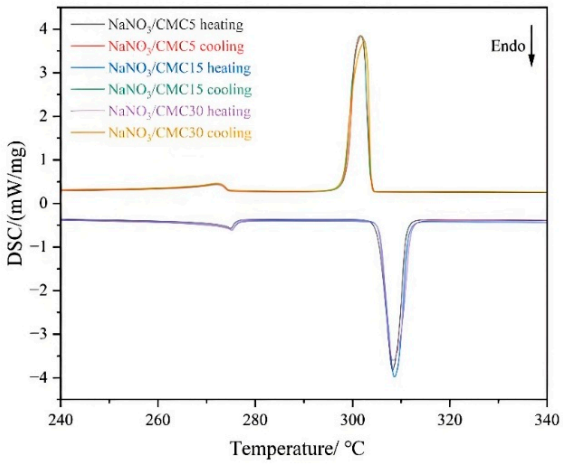


Figure 10. Heating and cooling DSC curves of the $NaNO_3$/CMC composites [141].

As shown in Figure 11, the composite material demonstrates excellent thermal stability. After undergoing 100 heating and thermal cycles, it can retain over 97% of its heat storage capacity. Additionally, the supercooling of $NaNO_3$/CMC composites is significantly reduced compared to pure $NaNO_3$, which aids in enhancing the stability of $NaNO_3$ and facilitating its large-scale application.

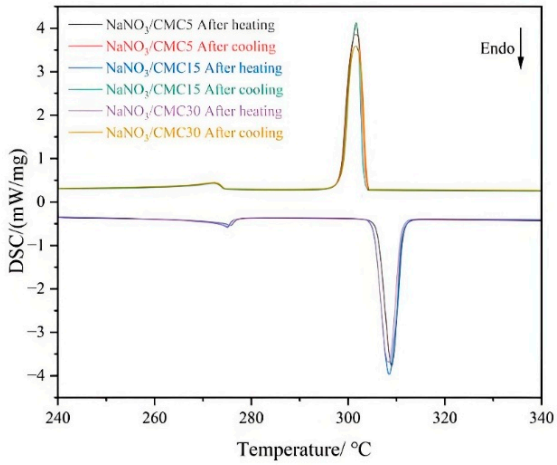


Figure 11. Heating and cooling DSC curves of the $NaNO_3$/CMC composites after thermal cycling [141].

Zhang et al. [105] utilized nickel slag and waste glass powder as raw materials to fabricate foam ceramics. Introducing nickel slag improved the bending strength and pore structure uniformity of the material, presenting a novel approach for recycling solid waste.

Liu et al. [143] synthesized anorthite–cordierite (AC) porous ceramics from steel SS, FNS, and FA. These porous ceramics, featuring high thermal conductivity, were developed as support frameworks for PCMs and show potential in high-temperature heat storage

applications like industrial waste heat recovery and solar energy storage. AC porous ceramics with varying phase compositions and corresponding $NaNO_3$/AC composite phase change materials (C-PCMs) were prepared using SS, FNS, and FA. As the cordierite phase content increased, the thermal conductivity of AC improved. AC0 exhibited a low thermal conductivity of 0.32 W/(m·K) and a high compressive strength of 22.5 MPa. These properties make it well-suited for use as a high-temperature kiln insulation material.

In summary, as a major solid waste, the excessive accumulation of nickel slag in China has posed significant treatment challenges. However, its enormous potential social and economic benefits have inspired extensive exploration by scholars. Nickel slag-based building materials have been widely used across the construction industry, effectively boosting nickel slag utilization. These innovations strongly support the sustainable development of China's metallurgical industry and establish a firm foundation for future theoretical research.

4.3. The Application of Lead Slag in Latent Heat Storage

Francis et al. [144] used DSC, SEM-EDS, XRD, Raman, and other analytical methods to investigate the crystallization mechanism of lead slag in glass–ceramic preparation, demonstrating the feasibility of using lead slag for this purpose. Pan et al. [145] designed glass–ceramics with lead slag as the primary raw material, incorporating waste glass and FA via a melting method. The resulting glass–ceramics came in various colors and met industrial standards, with leaching toxicity below regulatory limits. The iron and impurities in lead slag served as effective nucleating agents, enhancing the fixation of toxic elements within the glass–ceramic matrix. However, during the preparation of glass–ceramics from lead slag, strong nucleation drives rapid formation of a solid crystalline framework, causing a sharp increase in viscosity that hinders particle bonding. These factors cause the material to crystallize prematurely before sintering, leading to uneven surfaces in the final glass–ceramics [146–148].

Utilizing lead–zinc tailings and lead slag to make high-value glass–ceramics achieve comprehensive solid waste utilization and cuts landfill pollution from lead slag. First, borax and lead–zinc tailings were used to melt and temper lead slag, improving its sintering performance. At 1450 °C, lead slag with 40% lead–zinc tailings and 4% borax demonstrated good fluidity after melting and tempering. It was less likely to crystallize during water quenching, and the water-quenched slag exhibited excellent sintering properties. Next, the lead slag, lead–zinc tailings, and water-quenched slag obtained from borax smelting and tempering were milled, mixed with 10% albite, and sintered at 1050 °C for 90 min to prepare glass–ceramics. The glass–ceramics prepared exhibited outstanding properties: bulk density of 2.79 g/cm^3, water absorption of 0.05%, flexural strength of 102.18 MPa, acid resistance of 0.15%, and alkali resistance of 0.032%. Meanwhile, the leaching concentrations of Pb, Zn, As, and Cd were 0.125, 1.268, 0.324, and 0.029 mg/L, respectively, indicating strong resistance to heavy metal leaching. This study provides a new approach for the comprehensive utilization of solid waste.

4.4. Analysis and Comparisons for Latent Heat Storage

Analysis of research on non-ferrous metal slags, particularly copper, nickel, and lead slags, in latent heat storage reveals that:

(1) Copper Slag: It has extensive research and practical applications in the realm of sensible heat storage materials. Importantly, its role in latent heat storage applications has also gained significant attention. Research has demonstrated that through various modification techniques, including grinding, sieving, and heat treatment, the sensible heat storage performance of copper slag can be substantially enhanced. Moreover,

by integrating copper slag with other high-performance materials, it is possible to develop composite materials that exhibit remarkably improved thermal conductivity and heat storage capacity. These advancements not only broaden the application scope of copper slag in thermal energy storage but also offer innovative solutions for enhancing the efficiency of energy storage systems.

(2) Nickel Slag: As a major solid waste, the excessive accumulation of nickel slag in China poses significant disposal challenges. Yet, its potential social and economic benefits have spurred extensive scholarly exploration. Notably, studies on creating composite phase change thermal storage materials from nickel slag and other solid wastes have grown, achieving promising lab results that have improved nickel slag utilization. These innovations robustly underpin the sustainable development of China's metallurgical industry and solidify the foundation for future theoretical research.

(3) Lead Slag: Current research on lead slag shows limited direct applications in sensible and LHS. However, the above studies indicate that glass–ceramic materials prepared from lead slag possess both high-temperature resistance and excellent heavy metal leaching resistance, meeting the basic requirements for skeleton materials in high-temperature composite phase change heat storage materials. Specific applications in this field require further exploration.

5. Other Metallurgical Industry Waste

Naimi et al. [149] carried out an analysis of the chemical characteristics and thermal properties of electric arc furnace (EAF) slag, aluminum pot skimming (APS), ladle furnace (LF) slag, and aluminum white dross (AWD), with Figure 12 exhibiting sample photos. The potential of these materials as high-temperature sensible heat energy storage media was explored. The characterization outcomes demonstrated that the recovered samples are suitable for high-temperature TES applications at temperatures up to 1100 °C.



Figure 12. (**a**) Electric arc furnace slag, (**b**) ladle slag, (**c**) aluminum tank skimming slag, and (**d**) aluminum white slag [149].

Yang Wang et al. [77] performed thermodynamic analysis and friction property analysis on electric arc furnace (EAF) slags produced by two steel companies in China and Spain (sample photos are shown in Figure 13a and Figure 13b, respectively). The results showed that both slags remained stable below 1000 °C and exhibited a high heat capacity. The experimental specific heat capacity exhibited a temperature-dependent increase. For the Chinese EAF slag, it was 0.717 J/(g·K) at room temperature, 0.975 J/(g·K) at 500 °C, 0.713 J/(g·K) at room temperature (likely a repetition, possibly referring to the Spanish slag), and 0.858 J/(g·K) at 1000 °C for the other slag. At the test temperature, the thermal conductivity of both slags was 1.7 W/(m·K). The two slags showed outstanding wear resistance, making them suitable for heat energy storage systems.

Burcu et al. [150] analyzed and tested the pretreatment of demolition solid waste, revealing that the treated powder can be converted into a durable SHS material with high energy storage capacity, suitable for industrial solar energy storage applications at temperatures up to 700 °C.



(**a**) From a steel company in China (**b**) From a steel company in Spain

Figure 13. Electric arc furnace slag from a steel company in China and a steel company in Spain [77].

Agalit et al. [151] demonstrated that metallurgical slags and industrial byproducts like blast furnace slag, stainless stee and fly ash can function as SHS media. This is due to their outstanding thermal stability, high energy density, and economical cost.

Navarro et al. [100] investigated the heating and mechanical properties of mining and metallurgical industry byproducts as aggregates for solid sensible heat storage systems, aiming to identify alternative low-cost materials. The results indicated that these recycled materials hold great potential for TES applications. Materials with superior long-term storage performance, ranked in order, are WDF, cofalite [152] IB, and wrutf, which exhibit the highest energy density and lower costs. For short-term storage, WDF (a powder material generated during electric arc furnace steelmaking), salt rock minerals, concrete, wrutf (an ilmenite mining derivative primarily containing silicon oxide), cofalite, and IB (a chloride byproduct from potassium fertilizer production, mainly sodium chloride) perform well. The study concluded that WDF, IB, cofalite, and wrutf are the most cost-effective materials for these applications.

In summary, metallurgical slags possess significant potential for both sensible and latent heat storage applications.

6. Discussion

This study focuses on the composition, properties, and applications of non-ferrous metal smelting slags, particularly copper, nickel, and lead slags, in sensible and latent heat storage. Unlike other literature reviews that concentrate on specific aspects or single slag types, this study provides a more comprehensive summary of non-ferrous metal smelting wastes. It covers a broader variety of slags and emphasizes heat storage applications. This study is especially relevant for researchers exploring heat storage materials, as it reduces the need for extensive literature searches.

7. Conclusions and Prospect

This paper summarizes the properties, treatment methods and energy storage applications of various metal slags, with a focus on the particular uses of copper slag, nickel slag, lead slag, etc., in SHS and LHS. The following conclusions can be drawn:

(1) Metal slag is rich in a variety of metal elements or metal oxides, showing superior SHS performance, which makes it a research hotspot in the field of heat storage materials.

(2) Different metal slags can be blended with other slags to produce porous ceramic skeleton materials due to their varying oxides and metal elements. For instance, SS, FNS, and FA are utilized to create anorthite cordierite porous ceramics. Mixtures of lead slag, lead–zinc tailings, borax water-quenched slag, and albite form glass ceramics. Nickel slag combined with waste glass powder yields foam ceramics. Secondary

aluminum slag and FNS added to FA produce skeleton materials, while copper slag mixed with bauxite results in porous skeleton materials. These materials exhibit excellent thermal stability and mechanical properties, making them ideal for high-temperature thermal storage applications. Additionally, metal slags can be pressed into thermal insulation concrete bricks for building insulation, promoting energy conservation and environmental protection

(3) Although metal slag has broad application prospects in the field of heat storage, previous research shows that the application research of zinc slag, lead slag and other metal slag in the field of heat storage is still relatively scarce. Part of the research on slag mainly focuses on oxidation–reduction extraction and so on, but its potential in heat storage is still insufficient.

Prospects and suggestions for the future:

(1) The focus will be on the analysis of the components and properties of various metal slags, enhancing their energy storage capacity and thermal stability, and exploring novel processing techniques and additives.

(2) The pursuit of high cost effectiveness and eco-efficiency in slag-based energy storage systems involves applying new slag-based heat storage materials to renewable energy fields. This offers a novel research avenue for developing innovative materials with combined energy storage and other functional properties.

Author Contributions: Y.X.: Conceptualization, Methodology Writing—review and editing. M.Y.: Investigation, Extensive literature review, Writing—original draft, and Writing—review and editing. C.Z.: Supervision. Y.W.: Supervision. Y.Z.: Supervision. A.Z.: Review and editing. X.L.: I Review and editing. Y.D.: Supervision. All authors have read and agreed to the published version of the manuscript.

Funding: The authors are grateful for the financial support of the National Key Research and Development Program of China (No. 2022YFB2405202), the Scientific Research Program of the Beijing Municipal Education Commission (Grant NO. KM201910016011).

Conflicts of Interest: The authors declare that they have not known competing financial interests or personal relationships that could have appeared to influence the work reported in this paper.

References

1. Feng, P.H.; Zhao, B.C.; Wang, R.Z. Thermophysical heat storage for cooling, heating, and power generation: A review. *Appl. Therm. Eng.* **2020**, *166*, 114728. [CrossRef]
2. Gur, I.; Sawyer, K.; Prasher, R. Searching for a better thermal battery. *Science* **2012**, *335*, 1454–1455. [CrossRef] [PubMed]
3. Weber, R.; Gupta, A.K.; Mochida, S. High temperature air combustion (HiTAC): How it all started for applications in industrial furnaces and future prospects. *Appl. Energy* **2020**, *278*, 115551. [CrossRef]
4. Thonon, M.; Fraisse, G.; Zalewski, L.; Pailha, M. Simultaneous charging and discharging processes in latent heat thermal energy storage: A review. *Therm. Sci. Eng. Prog.* **2024**, *47*, 102299. [CrossRef]
5. Xiong, Y.; Zhang, A.; Zhao, Y.; Xu, Q.; Ding, Y. A Mini Review on Sewage Sludge and Red Mud Recycling for Thermal Energy Storage. *Energies* **2024**, *17*, 2079. [CrossRef]
6. Carrillo, A.J.; Gonzalez-Aguilar, J.; Romero, M.; Coronado, J.M. Solar Energy on Demand: A Review on High Temperature Thermochemical Heat Storage Systems and Materials. *Chem. Rev.* **2019**, *119*, 4777–4816. [CrossRef]
7. Liu, M.; Saman, W.; Bruno, F. Review on storage materials and thermal performance enhancement techniques for high temperature phase change thermal storage systems. *Renew. Sustain. Energy Rev.* **2012**, *16*, 2118–2132. [CrossRef]
8. Asegun Henry, R.P. The Prospect of High Temperature Solid State Energy Conversion to reduce the cost of concentrated solar power. *Energy Environ. Sci.* **2014**, *7*, 1819–1828. [CrossRef]
9. Zhao, Y.; Zhao, C.Y.; Markides, C.N.; Wang, H.; Li, W. Medium- and high-temperature latent and thermochemical heat storage using metals and metallic compounds as heat storage media: A technical review. *Appl. Energy* **2020**, *280*, 115950. [CrossRef]
10. Kumar, L.; Hasanuzzaman, M.; Rahim, N.A. Global advancement of solar thermal energy technologies for industrial process heat and its future prospects: A review. *Energy Convers. Manag.* **2019**, *195*, 885–908. [CrossRef]

11. Yang, C.Y.; Reijonen, I.; Yu, H.; Dharmarajan, R.; Seshadri, B.; Bolan, N.S. Back to _basic slags as a phosphorous source and liming material. In *Soil Amendments For Sustainability: Challenges and Perspectives*; CRC Press, Taylor & Francis Group: Boca Raton, FL, USA, 2018.
12. Seetharaman, S.; Guthrie, R.; McLean, A.; Seetharaman, S.; Sohn, H.Y. *Treatise on Process Metallurgy*; Elsevier: Amsterdam, The Netherlands, 2013; Volume 3: Industrial Processer.
13. US Geological Survey. Mineral Commodity Summaries: Iron and Steel Slag. 2025. Available online: https://www.usgs.gov/centers/nmic/iron-and-steel-slag-statistics-and-information?qt-science_support_page_related_con=0#qt-science_support_page_related_con (accessed on 3 July 2025).
14. Biava, G.; Depero, L.E.; Bontempi, E. Accelerated Carbonation of Steel Slag and Their Valorisation in Cement Products: A Review. *Span. J. Soil Sci.* **2024**, *14*, 12908. [CrossRef]
15. Gao, W.; Zhou, W.; Lyu, X.; Liu, X.; Su, H.; Li, C.; Wang, H. Comprehensive utilization of steel slag: A review. *Powder Technol.* **2023**, *422*, 118449. [CrossRef]
16. Klaffenbach, E.; Montenegro, V.; Guo, M.; Blanpain, B. Sustainable and Comprehensive Utilization of Copper Slag: A Review and Critical Analysis. *J. Sustain. Metall.* **2023**, *9*, 468–496. [CrossRef]
17. Tian, H.; Guo, Z.; Pan, J.; Zhu, D.; Yang, C.; Xue, Y.; Li, S.; Wang, D. Comprehensive review on metallurgical recycling and cleaning of copper slag. *Resour. Conserv. Recycl.* **2021**, *168*, 105366. [CrossRef]
18. Madheswaran, C.K.; Ambily, P.S.; Dattatreya, J.K.; Rajamane, N.P. Studies on use of Copper Slag as Replacement Material for River Sand in Building Constructions. *J. Inst. Eng. (India) Ser. A* **2014**, *95*, 169–177. [CrossRef]
19. Shen, H.; Forssberg, E. An overview of recovery of metals from slags. *Waste Manag.* **2003**, *23*, 933–949. [CrossRef]
20. Gorai, B.; Jana, R.K.; Premchand. Characteristics and utilisation of copper slag—A review. *Resour. Conserv. Recycl.* **2003**, *39*, 299–313. [CrossRef]
21. González, C.; Parra, R.; Klenovcanova, A.; Imris, I.; Sánchez, M. Reduction of Chilean copper slags: A case of waste management project. *Scand. J. Metall.* **2005**, *34*, 143–149. [CrossRef]
22. Edraki, M.; Baumgartl, T.; Manlapig, E.; Bradshaw, D.; Franks, D.M.; Moran, C.J. Designing mine tailings for better environmental, social and economic outcomes: A review of alternative approaches. *J. Clean. Prod.* **2014**, *84*, 411–420. [CrossRef]
23. Phiri, T.C.; Singh, P.; Nikoloski, A.N. The potential for copper slag waste as a resource for a circular economy: A review—Part II. *Miner. Eng.* **2021**, *172*, 107150. [CrossRef]
24. Busolic, D.; Parada, F.; Parra, R.; Sanchez, M.; Palacios, J.; Hino, M. Recovery of iron from copper flash smelting slags. *Miner. Process. Extr. Metall.* **2013**, *120*, 32–36. [CrossRef]
25. Bulut, G. Recovery of copper and cobalt from ancient slag. *Waste Manag. Res.* **2006**, *24*, 118–124. [CrossRef] [PubMed]
26. Gabasiane, T.S.; Danha, G.; Mamvura, T.A.; Mashifana, T.; Dzinomwa, G. Environmental and Socioeconomic Impact of Copper Slag—A Review. *Crystals* **2021**, *11*, 1504. [CrossRef]
27. Alp, I.; Deveci, H.; Sungun, H. Utilization of flotation wastes of copper slag as raw material in cement production. *J. Hazard. Mater.* **2008**, *159*, 390–395. [CrossRef]
28. Rasoul Abdar Esfahani, S.M.; Zareei, S.A.; Madhkhan, M.; Ameri, F.; Rashidiani, J.; Taheri, R.A. Mechanical and gamma-ray shielding properties and environmental benefits of concrete incorporating GGBFS and copper slag. *J. Build. Eng.* **2021**, *33*, 101615. [CrossRef]
29. Sridharan, M.; Madhavi, T.C. Investigating the influence of copper slag on the mechanical behaviour of concrete. *Mater. Today Proc.* **2021**, *46*, 3225–3232. [CrossRef]
30. Al-Jabri, K.S.; Al-Saidy, A.H.; Taha, R. Effect of copper slag as a fine aggregate on the properties of cement mortars and concrete. *Constr. Build. Mater.* **2011**, *25*, 933–938. [CrossRef]
31. Potysz, A.; van Hullebusch, E.D.; Kierczak, J.; Grybos, M.; Lens, P.N.L.; Guibaud, G. Copper Metallurgical Slags—Current Knowledge and Fate: A Review. *Crit. Rev. Environ. Sci. Technol.* **2015**, *45*, 2424–2488. [CrossRef]
32. Kundu, T.; Senapati, S.; Das, S.K.; Angadi, S.I.; Rath, S.S. A comprehensive review on the recovery of copper values from copper slag. *Powder Technol.* **2023**, *426*, 118693. [CrossRef]
33. Coelho, L.M.; Guimarães, A.C.R.; Alves Moreira, C.R.C.L.; dos Santos, G.P.P.; Monteiro, S.N.; da Silveira, P.H.P.M. Feasibility of Using Ferronickel Slag as a Sustainable Alternative Aggregate in Hot Mix Asphalt. *Sustainability* **2024**, *16*, 8642. [CrossRef]
34. Yanning, S.; Qiao, H.; Qiong, F.; Chao, W.; Jianghua, Z. Application of metallurgical ferronickel slag in building materials: A review. *J. Build. Eng.* **2024**, *96*, 110632. [CrossRef]
35. Wang, D.; Ma, B.; Pang, L.; Wang, Q. Alkali-activated blast furnace ferronickel slag for Cr immobilization. *Cem. Concr. Compos.* **2024**, *150*, 105560. [CrossRef]
36. Xi, B.; Li, R.; Zhao, X.; Dang, Q.; Zhang, D.; Tan, W. Constraints and opportunities for the recycling of growing ferronickel slag in China. *Resour. Conserv. Recycl.* **2018**, *139*, 15–16. [CrossRef]
37. Nguyen, Q.D.; Castel, A.; Kim, T.; Khan, M.S.H. Performance of fly ash concrete with ferronickel slag fine aggregate against alkali-silica reaction and chloride diffusion. *Cem. Concr. Res.* **2021**, *139*, 106265. [CrossRef]

38. Gu, Y.-c.; Li, J.-L.; Peng, J.-K.; Xing, F.; Long, W.-J.; Khayat, K.H. Immobilization of hazardous ferronickel slag treated using ternary limestone calcined clay cement. *Constr. Build. Mater.* **2020**, *250*, 118837. [CrossRef]
39. Nowinska, K.; Adamczyk, Z. Zinc and Lead Metallurgical Slags as a Potential Source of Metal Recovery: A Review. *Materials* **2023**, *16*, 7295. [CrossRef]
40. Pan, D.a.; Li, L.; Tian, X.; Wu, Y.; Cheng, N.; Yu, H. A review on lead slag generation, characteristics, and utilization. *Resour. Conserv. Recycl.* **2019**, *146*, 140–155. [CrossRef]
41. Sun, Y.; Hu, S.; Zhang, P.; Elmaadawy, K.; Ke, Y.; Li, J.; Li, M.; Hu, J.; Liu, B.; Yang, J.; et al. Microwave enhanced solidification/stabilization of lead slag with fly ash based geopolymer. *J. Clean. Prod.* **2020**, *272*, 122957. [CrossRef]
42. Tukker, A.; Buist, H.; van Oers, L.; van der Voet, E. Risks to health and environment of the use of lead in products in the EU. *Resour. Conserv. Recycl.* **2006**, *49*, 89–109. [CrossRef]
43. Mor, S.; Ravindra, K.; Dahiyaa, R.P.; Chandra, A. Leachate Characterization and assessment of groundwater pollution near municipal solid waste landfill site. *Environ. Monit. Assess.* **2006**, *118*, 435–456. [CrossRef]
44. Hilts, S.R. Effect of smelter emission reductions on children's blood lead levels. *Sci. Total Environ.* **2003**, *303*, 51–58. [CrossRef] [PubMed]
45. Ogundiran, M.B.; Ogundele, D.T.; Afolayan, P.G.; Osibanjo, O. Heavy Metals Levels in Forage Grasses, Leachate and Lactating CowsReared around Lead Slag Dumpsites in Nigeria. *Int. J. Environ. Res.* **2012**, *63*, 695–702.
46. Saca, N.; Radu, L.; Fugaru, V.; Gheorghe, M.; Petre, I. Composite materials with primary lead slag content: Application in gamma radiation shielding and waste encapsulation fields. *J. Clean. Prod.* **2018**, *179*, 255–265. [CrossRef]
47. Yan, P.; Chen, B.; Aminul Haque, M.; Liu, T. Influence of red mud on the engineering and microstructural properties of sustainable ultra-high performance concrete. *Constr. Build. Mater.* **2023**, *396*, 132404. [CrossRef]
48. Liu, X.; Han, Y.; He, F.; Gao, P.; Yuan, S. Characteristic, hazard and iron recovery technology of red mud—A critical review. *J. Hazard. Mater.* **2021**, *420*, 126542. [CrossRef]
49. Wu, P.; Liu, X.; Zhang, Z.; Wei, C. Properties of red mud-filled and modified resin composites. *Constr. Build. Mater.* **2023**, *409*, 133984. [CrossRef]
50. Xue, S.; Li, M.; Jiang, J.; Millar, G.J.; Li, C.; Kong, X. Phosphogypsum stabilization of bauxite residue: Conversion of its alkaline characteristics. *J. Environ. Sci.* **2019**, *77*, 1–10. [CrossRef]
51. Liu, S.; Liu, Z.; Zhu, H.; Wang, Z.; Guo, J.; Zhang, X.; Yu, H.; Yue, X.; Ning, P.; Li, B. The roles of red mud as desulfurization and denitrification in flue gas: A review. *J. Environ. Chem. Eng.* **2023**, *11*, 109770. [CrossRef]
52. Nganda, A.; Srivastava, P.; Lamba, B.Y.; Pandey, A.; Kumar, M. Advances in the fabrication, modification, and performance of biochar, red mud, calcium oxide, and bentonite catalysts in waste-to-fuel conversion. *Environ. Res.* **2023**, *232*, 116284. [CrossRef]
53. Occhicone, A.; Graziuso, S.G.; De Gregorio, E.; Montagnaro, F.; Ricciotti, L.; Tarallo, O.; Roviello, G.; Ferone, C. Synthesis and characterization of new acid-activated red mud-metakaolin geopolymers and comparison with their alkaline counterparts. *J. Clean. Prod.* **2024**, *435*, 140492. [CrossRef]
54. Chen, J.; Wang, Y.; Liu, Z. Red mud-based catalysts for the catalytic removal of typical air pollutants: A review. *J. Environ. Sci.* **2023**, *127*, 628–640. [CrossRef] [PubMed]
55. de Sousa Cordeiro, E.; Scaratti, G.; de Souza, D.C.S.; Nickel, C.D.M.; José, H.J.; de Fátima Peralta Muniz Moreira, R.; De Noni, A. Red mud as catalyst for the treatment of pharmaceuticals compounds by advanced oxidation processes—A review. *Environ. Nanotechnol. Monit. Manag.* **2024**, *21*, 100938. [CrossRef]
56. Zhang, J.; Yao, Z.; Wang, K.; Wang, F.; Jiang, H.; Liang, M.; Wei, J.; Airey, G. Sustainable utilization of bauxite residue (Red Mud) as a road material in pavements: A critical review. *Constr. Build. Mater.* **2021**, *270*, 121419. [CrossRef]
57. Yang, X.; Zhao, J.; Li, H.; Zhao, P.; Chen, Q. Recycling red mud from the production of aluminium as a red cement-based mortar. *Waste Manag. Res.* **2017**, *35*, 500–507. [CrossRef]
58. Ke, W.; Li, C.; Zhu, F.; Luo, X.; Feng, J.; Li, X.; Jiang, Y.; Wu, C.; Hartley, W.; Xue, S. Effect of potentially toxic elements on soil multifunctionality at a lead smelting site. *J. Hazard. Mater.* **2023**, *454*, 131525. [CrossRef]
59. Yang, S.; Yao, X.; Li, J.; Wang, X.; Zhang, C.; Wu, S.; Wang, K.; Wang, W. Preparation and properties of ready-to-use low-density foamed concrete derived from industrial solid wastes. *Constr. Build. Mater.* **2021**, *287*, 122946. [CrossRef]
60. Ren, C.; Wang, W.; Li, G. Preparation of high-performance cementitious materials from industrial solid waste. *Constr. Build. Mater.* **2017**, *152*, 39–47. [CrossRef]
61. Liu, Y.; Guo, D.; Dong, L.; Xu, Y.; Liu, J. Pollution Status and Environmental Sound Management (ESM) Trends on Typical General Industrial Solid Waste. *Procedia Environ. Sci.* **2016**, *31*, 615–620. [CrossRef]
62. Ananth, S.; Selvakumar, P. Experimental investigation of sand-based sensible heat energy storage system. *Appl. Therm. Eng.* **2025**, *264*, 125390. [CrossRef]
63. Abubakar, S.; Umaru, S.; Kaisan, M.U.; Umar, U.A.; Ashok, B.; Nanthagopal, K. Development and performance comparison of mixed-mode solar crop dryers with and without thermal storage. *Renew. Energy* **2018**, *128*, 285–298. [CrossRef]

64. Kedida, D.K.; Amibe, D.A.; Birhane, Y.T. Performance of a Pebble Bed Thermal Storage Integrated with Concentrating Parabolic Solar Collector for Cooking. *J. Renew. Energy* **2019**, *2019*, 4238549. [CrossRef]
65. Wang, S.; Abdulridha, A.; Naito, C.; Quiel, S.; Suleiman, M.; Romero, C.; Neti, S. Enhancement of conventional concrete mix designs for sensible thermal energy storage applications. *J. Energy Storage* **2023**, *61*, 106735. [CrossRef]
66. Lakshmi, D.V.N.; Layek, A.; Kumar, P.M. Performance Analysis of Trapezoidal Corrugated Solar Air Heater with Sensible Heat Storage Material. *Energy Procedia* **2017**, *109*, 463–470. [CrossRef]
67. Hu, B.; Wang, H.; Yang, J.; Li, J.; Li, C.; Ren, X. Experimental and numerical investigation on heating performance comparison of air conditioning heating systems based on water-phase change material heat storage system and water heat storage system. *Energy* **2025**, *331*, 137005. [CrossRef]
68. Mehla, N.; Kumar, A. Experimental evaluation of used engine oil based thermal energy storage coupled with novel evacuated tube solar air collector (NETAC). *J. Energy Storage* **2021**, *39*, 102656. [CrossRef]
69. Ndukwu, M.C.; Onyenwigwe, D.; Abam, F.I.; Eke, A.B.; Dirioha, C. Development of a low-cost wind-powered active solar dryer integrated with glycerol as thermal storage. *Renew. Energy* **2020**, *154*, 553–568. [CrossRef]
70. Sharma, A.; Tyagi, V.V.; Chen, C.R.; Buddhi, D. Review on thermal energy storage with phase change materials and applications. *Renew. Sustain. Energy Rev.* **2009**, *13*, 318–345. [CrossRef]
71. Ganapathiraman, S.; Manickam, P. Experimental studies on evacuated tube collector with in-built energy storage—Waste car engine oil as sensible heat storage medium. *J. Energy Storage* **2024**, *84*, 110929. [CrossRef]
72. Abddaim, E.; Sakami, S.; El Hassnaoui, A.; Boukhattem, L. Impact of temperature on chemical, thermo-physical, and mechanical properties of four rock materials for sensible thermal energy storage. *J. Energy Storage* **2024**, *89*, 111602. [CrossRef]
73. Grirate, H.; Agalit, H.; Zari, N.; Elmchaouri, A.; Molina, S.; Couturier, R. Experimental and numerical investigation of potential filler materials for thermal oil thermocline storage. *Sol. Energy* **2016**, *131*, 260–274. [CrossRef]
74. Liu, J.; Chang, Z.; Wang, L.; Xu, J.; Kuang, R.; Wu, Z. Exploration of Basalt Glasses as High-Temperature Sensible Heat Storage Materials. *ACS Omega* **2020**, *5*, 19236–19246. [CrossRef] [PubMed]
75. Santos, A.; Almeida, F.; Neto, F. Development of rock sensible heat storage system: Modeling of a hematite reservoir. *J. Energy Storage* **2021**, *40*, 102818. [CrossRef]
76. Khare, S.; Dell'Amico, M.; Knight, C.; McGarry, S. Selection of materials for high temperature sensible energy storage. *Sol. Energy Mater. Sol. Cells* **2013**, *115*, 114–122. [CrossRef]
77. Wang, Y.; Wang, Y.; Li, H.; Zhou, J.; Cen, K. Thermal properties and friction behaviors of slag as energy storage material in concentrate solar power plants. *Sol. Energy Mater. Sol. Cells* **2018**, *182*, 21–29. [CrossRef]
78. Zhang, J.; Guo, Z.; Zhu, Y.; Zhang, H.; Yan, M.; Liu, D.; Hao, J. Preparation and characterization of novel low-cost sensible heat storage materials with steel slag. *J. Energy Storage* **2024**, *76*, 109643. [CrossRef]
79. Fang, Y.; Wang, K.; Ding, Y.; Liang, X.; Wang, S.; Gao, X.; Zhang, Z. Fabrication and thermal properties of $CaCl_2 \cdot 6H_2O$–$CO(NH_2)_2/SiO_2$ as room-temperature shape-stable composite PCM for building thermal insulation. *Sol. Energy Mater. Sol. Cells* **2021**, *232*, 111355. [CrossRef]
80. Harikrishnan, S.; Devaraju, A.; Sivasamy, P.; Kalaiselvam, S. Experimental Investigation of Improved Thermal Characteristics of SiO_2/myristic acid Nanofluid as Phase Change Material (PCM). *Mater. Today Proc.* **2019**, *9*, 397–409. [CrossRef]
81. Yoo, D.H.; Jeon, I.K.; Kim, H.G.; Lee, J.S.; Ryou, J.-S. Experimental evaluation of fire resistance performance of cement mortar with PCM/$Mg(OH)_2$-based composite fine aggregate. *Constr. Build. Mater.* **2021**, *287*, 123018. [CrossRef]
82. Yu, Q.; Jiang, Z.; Cong, L.; Lu, T.; Suleiman, B.; Leng, G.; Wu, Z.; Ding, Y.; Li, Y. A novel low-temperature fabrication approach of composite phase change materials for high temperature thermal energy storage. *Appl. Energy* **2019**, *237*, 367–377. [CrossRef]
83. Chai, Z.; Chen, X.; Fang, M.; Min, X.; Huang, Z.; Wang, Q.; Liu, C.; Liu, Y.; Huang, F. Fabrication and properties of high-thermal-storage RTO ceramics using bauxite tailings and red mud. *Ceram. Int.* **2023**, *49*, 31342–31350. [CrossRef]
84. Jeong, S.-G.; Jeon, J.; Lee, J.-H.; Kim, S. Optimal preparation of PCM/diatomite composites for enhancing thermal properties. *Int. J. Heat Mass Transf.* **2013**, *62*, 711–717. [CrossRef]
85. Xiao, J.; Huang, J.; Zhu, P.; Wang, C.; Li, X. Preparation, characterization and thermal properties of binary nitrate salts/expanded graphite as composite phase change material. *Thermochim. Acta* **2014**, *587*, 52–58. [CrossRef]
86. Dora, S.; Mini, K.M. Performance assessment of capric acid-ethyl alcohol/expanded vermiculite phase change material incorporated cement mortar for thermal insulation in buildings. *J. Energy Storage* **2023**, *72*, 108550. [CrossRef]
87. Wang, Y.; Qin, Z.; Zhang, T.; Zhang, D. Preparation and thermophysical properties of three-dimensional attapulgite based composite phase change materials. *J. Energy Storage* **2020**, *32*, 101847. [CrossRef]
88. Buonomo, B.; Rita Golia, M.; Manca, O.; Nardini, S. A review on thermal energy storage with phase change materials enhanced by metal foams. *Therm. Sci. Eng. Prog.* **2024**, *53*, 102732. [CrossRef]
89. Sun, J.; Zhao, J.; Zhang, W.; Xu, J.; Wang, B.; Wang, X.; Zhou, J.; Guo, H.; Liu, Y. Composites with a Novel Core–shell Structural Expanded Perlite/Polyethylene glycol Composite PCM as Novel Green Energy Storage Composites for Building Energy Conservation. *Appl. Energy* **2023**, *330*, 120363. [CrossRef]

90. Ren, Y.; Xu, C.; Yuan, M.; Ye, F.; Ju, X.; Du, X. $Ca(NO_3)_2$-$NaNO_3$/expanded graphite composite as a novel shape-stable phase change material for mid- to high-temperature thermal energy storage. *Energy Convers. Manag.* **2018**, *163*, 50–58. [CrossRef]
91. Wen, R.; Xu, Y.; Xu, Y.; Sun, Z.; Zhang, L.; Qiao, J.; Wu, X.; Min, X.; Huang, Z. Attapulgite: A promising natural mineral as carrier material for fatty acids phase change material. *J Therm Anal Calorim* **2022**, *147*, 7203–7212. [CrossRef]
92. Soleimanpour, S.; Sadrameli, S.M.; Mousavi, S.A.H.S.; Jafaripour, M. Preparation and characterization of high temperature shape stable $NaNO_3$/diatomite phase change materials with nanoparticles for solar energy storage applications. *J. Energy Storage* **2022**, *45*, 103735. [CrossRef]
93. Rathore, P.K.S.; Shukla, S.k. Improvement in thermal properties of PCM/Expanded vermiculite/expanded graphite shape stabilized composite PCM for building energy applications. *Renew. Energy* **2021**, *176*, 295–304. [CrossRef]
94. Xiong, Y.; Fan, Y.; Wu, Y.; Ren, J.; Li, X.; Yao, C.; Zhao, Y.; Xu, Q.; Ding, Y. Low-carbon shape-stable phase change composite utilizing semi-coke ash for building thermal energy storage. *Sol. Energy Mater. Sol. Cells* **2024**, *270*, 112823. [CrossRef]
95. Xiong, Y.; Yang, Y.; Zhang, A.; Ren, J.; Xu, Q.; Wu, Y.; Zhao, Y.; Ding, Y. Investigation on low-carbon shape-stable phase change composite by steel slag and carbide slag for solar thermal energy storage. *J. Energy Storage* **2024**, *76*, 109736. [CrossRef]
96. Zheng, W.; He, D.; Wang, Y.; Chen, J.; Xue, M.; Li, H. Preparation of cement-based color facing mortar by copper pyrometallurgical slag modification: Efficient utilization of high-iron-content slag. *J. Environ. Chem. Eng.* **2021**, *9*, 105888. [CrossRef]
97. Li, Z.; Ma, G.; Zheng, D.; Zhang, X. Effect of Fe_2O_3 on the crystallization behavior, microstructure and properties of glass-ceramics prepared from the modified tailings after reduction of copper slag. *Mater. Today Commun.* **2022**, *31*, 103516. [CrossRef]
98. Heo, J.H.; Kim, B.-S.; Park, J.H. Effect of CaO Addition on Iron Recovery from Copper Smelting Slags by Solid Carbon. *Metall. Mater. Trans. B* **2013**, *44*, 1352–1363. [CrossRef]
99. Calderón-Vásquez, I.; Segovia, V.; Cardemil, J.M.; Barraza, R. Assessing the use of copper slags as thermal energy storage material for packed-bed systems. *Energy* **2021**, *227*, 120370. [CrossRef]
100. Navarro, M.E.; Martínez, M.; Gil, A.; Fernández, A.I.; Cabeza, L.F.; Olives, R.; Py, X. Selection and characterization of recycled materials for sensible thermal energy storage. *Sol. Energy Mater. Sol. Cells* **2012**, *107*, 131–135. [CrossRef]
101. Ortega, I.; Faik, A.; Gil, A.; Rodríguez-Aseguinolaza, J.; D'Aguanno, B. Thermo-physical Properties of a Steel-making by-product to be used as Thermal Energy Storage Material in a Packed-bed System. *Energy Procedia* **2015**, *69*, 968–977. [CrossRef]
102. Ortega-Fernández, I.; Calvet, N.; Gil, A.; Rodríguez-Aseguinolaza, J.; Faik, A.; D'Aguanno, B. Thermophysical characterization of a by-product from the steel industry to be used as a sustainable and low-cost thermal energy storage material. *Energy* **2015**, *89*, 601–609. [CrossRef]
103. Li, X.; Zhang, X.; Zang, X.; Xing, X. Structure and Phase Changes of Nickel Slag in Oxidation Treatment. *Minerals* **2020**, *10*, 313. [CrossRef]
104. Hussain, A.; Abidi, I.H.; Tso, C.Y.; Chan, K.C.; Luo, Z.; Chao, C.Y.H. Thermal management of lithium ion batteries using graphene coated nickel foam saturated with phase change materials. *Int. J. Therm. Sci.* **2018**, *124*, 23–35. [CrossRef]
105. Zhang, C.; Wang, X.; Zhu, H.; Wu, Q.; Hu, Z.; Feng, Z.; Jia, Z. Preparation and properties of foam ceramic from nickel slag and waste glass powder. *Ceram. Int.* **2020**, *46*, 23623–23628. [CrossRef]
106. Liu, J.; Xu, J.; Zhang, Y.; Su, Z.; Xu, C.; Jiang, T. Co-utilization of secondary aluminum dross and ferronickel slag for preparation of cordierite–mullite insulating ceramic. *J. Am. Ceram. Soc.* **2022**, *106*, 2049–2060. [CrossRef]
107. Chen, S.; Chen, F.; Zheng, C.; Wu, Z. Dynamic mechanical properties of ferronickel slag powder-modified soil-cement using split-hopkinson pressure bar testing. *Mater. Res. Express* **2023**, *10*, 115503. [CrossRef]
108. Liu, P.; Li, B.; Cheung, S.C.P.; Wu, W. Material and energy flows in rotary kiln-electric furnace smelting of ferronickel alloy with energy saving. *Appl. Therm. Eng.* **2016**, *109*, 542–559. [CrossRef]
109. Choi, Y.C.; Choi, S. Alkali–silica reactivity of cementitious materials using ferro-nickel slag fine aggregates produced in different cooling conditions. *Constr. Build. Mater.* **2015**, *99*, 279–287. [CrossRef]
110. Huang, Y.; Wang, Q.; Shi, M. Characteristics and reactivity of ferronickel slag powder. *Constr. Build. Mater.* **2017**, *156*, 773–789. [CrossRef]
111. Cao, R.; Jia, Z.; Zhang, Z.; Zhang, Y.; Banthia, N. Leaching kinetics and reactivity evaluation of ferronickel slag in alkaline conditions. *Cem. Concr. Res.* **2020**, *137*, 106202. [CrossRef]
112. Komnitsas, K.; Zaharaki, D.; Bartzas, G. Effect of sulphate and nitrate anions on heavy metal immobilisation in ferronickel slag geopolymers. *Appl. Clay Sci.* **2013**, *73*, 103–109. [CrossRef]
113. Wang, M.; Feng, C.; Liu, Y.; Zhang, D.; Xiong, D.; Zhang, X. Enhancement of pozzolanic activity of high-magnesium nickel slag via phase separation by adding CaO. *Mater. Today Commun.* **2023**, *34*, 105427. [CrossRef]
114. Huang, Z.; Wang, Q.; Lu, J. The effects of cations and concentration on reaction mechanism of alkali-activated blast furnace ferronickel slag. *Compos. Part B Eng.* **2022**, *236*, 109825. [CrossRef]
115. Wang, D.; Wang, Q.; Zhuang, S.; Yang, J. Evaluation of alkali-activated blast furnace ferronickel slag as a cementitious material: Reaction mechanism, engineering properties and leaching behaviors. *Constr. Build. Mater.* **2018**, *188*, 860–873. [CrossRef]

116. Yanning, S.; Qiong, F.; Hongxia, Q.; Chao, W. Study on mechanically activated ferrous extraction tailing of nickel slag as cementitious materials: Physical and chemical properties, mechanical properties and reaction mechanism. *Constr. Build. Mater.* **2024**, *422*, 135748. [CrossRef]
117. Sobanska, S.; Deneele, D.; Barbillat, J.; Ledésert, B. Natural weathering of slags from primary Pb–Zn smelting as evidenced by Raman microspectroscopy. *Appl. Geochem.* **2016**, *64*, 107–117. [CrossRef]
118. Scheinert, M.; Kupsch, H.; Bletz, B. Geochemical investigations of slags from the historical smelting in Freiberg, Erzgebirge (Germany). *Geochemistry* **2009**, *69*, 81–90. [CrossRef]
119. de Andrade Lima, L.R.P.; Bernardez, L.A. Characterization of the lead smelter slag in Santo Amaro, Bahia, Brazil. *J. Hazard. Mater.* **2011**, *189*, 692–699. [CrossRef]
120. Ettler, V.; Komarkova, M.; Jehlicka, J.; Coufal, P.; Hradil, D.; Machovic, V.; Delorme, F. Leaching of lead metallurgical slag in citric solutions--implications for disposal and weathering in soil environments. *Chemosphere* **2004**, *57*, 567–577. [CrossRef]
121. Seignez, N.; Gauthier, A.; Bulteel, D.; Buatier, M.; Recourt, P.; Damidot, D.; Potdevin, J.L. Effect of Pb-rich and Fe-rich entities during alteration of a partially vitrified metallurgical waste. *J. Hazard. Mater.* **2007**, *149*, 418–431. [CrossRef]
122. Seignez, N.; Gauthier, A.; Bulteel, D.; Damidot, D.; Potdevin, J.-L. Leaching of lead metallurgical slags and pollutant mobility far from equilibrium conditions. *Appl. Geochem.* **2008**, *23*, 3699–3711. [CrossRef]
123. Ettler, V.; Johan, Z.; Kříbek, B.; Šebek, O.; Mihaljevič, M. Mineralogy and environmental stability of slags from the Tsumeb smelter, Namibia. *Appl. Geochem.* **2009**, *24*, 1–15. [CrossRef]
124. de Andrade Lima, L.R.P.; Bernardez, L.A. Evaluation of the chemical stability of a landfilled primary lead smelting slag. *Environ. Earth Sci.* **2012**, *68*, 1033–1040. [CrossRef]
125. Ettler, V.; Johan, Z. 12 years of leaching of contaminants from Pb smelter slags: Geochemical/mineralogical controls and slag recycling potential. *Appl. Geochem.* **2014**, *40*, 97–103. [CrossRef]
126. Yin, N.H.; Sivry, Y.; Guyot, F.; Lens, P.N.; van Hullebusch, E.D. Evaluation on chemical stability of lead blast furnace (LBF) and imperial smelting furnace (ISF) slags. *J. Environ. Manag.* **2016**, *180*, 310–323. [CrossRef] [PubMed]
127. Onisei, S.; Pontikes, Y.; Van Gerven, T.; Angelopoulos, G.N.; Velea, T.; Predica, V.; Moldovan, P. Synthesis of inorganic polymers using fly ash and primary lead slag. *J. Hazard. Mater.* **2012**, *205–206*, 101–110. [CrossRef]
128. Segovia, A.V.; Cardemil, J.M.; Sancy, M.; Escobar, R. Analysis of copper slag from a Chilean foundry for application as filler material in thermal energy storage systems. *J. Energy Storage* **2025**, *111*, 115281. [CrossRef]
129. Sibarani, D.; Hamuyuni, J.; Luomala, M.; Lindgren, M.; Jokilaakso, A. Thermal Conductivity of Solidified Industrial Copper Matte and Fayalite Slag. *JOM* **2020**, *72*, 1927–1934. [CrossRef]
130. Khare, S.; Dell'Amico, M.; Knight, C.; McGarry, S. Selection of materials for high temperature latent heat energy storage. *Sol. Energy Mater. Sol. Cells* **2012**, *107*, 20–27. [CrossRef]
131. Zhang, C.; Zhu, B.; Wu, Q.; Li, Y.; Feng, Z.; Wang, Y.; Hu, Z. Physical properties and microstructure of nickel slag/metakaolin-based geopolymer with different contents of nickel slag. *Adv. Cem. Res.* **2020**, *32*, 244–250. [CrossRef]
132. Buzatu, T.; Talpoş, E.; Petrescu, M.I.; Ghica, V.G.; Iacob, G.; Buzatu, M. Utilization of granulated lead slag as a structural material in roads constructions. *J. Mater. Cycles Waste Manag.* **2014**, *17*, 707–717. [CrossRef]
133. Barna, R.; Moszkowicz, P.; Gervais, C. Leaching assessment of road materials containing primary lead and zinc slags. *Waste Manag.* **2004**, *24*, 945–955. [CrossRef]
134. Carvalho, S.Z.; Vernilli, F.; Almeida, B.; Demarco, M.; Silva, S.N. The recycling effect of BOF slag in the portland cement properties. *Resour. Conserv. Recycl.* **2017**, *127*, 216–220. [CrossRef]
135. Alwaeli, M. Application of granulated lead–zinc slag in concrete as an opportunity to save natural resources. *Radiat. Phys. Chem.* **2013**, *83*, 54–60. [CrossRef]
136. Atzeni, C.; Massidda, L.; Sanna, U. Use of granulated slag from lead and zinc processing in concrete technology. *Cem. Concr. Res.* **1996**, *26*, 1381–1388. [CrossRef]
137. Pelino, M. Recycling of zinc-hydrometallurgy wastes in glass and glass ceramic materials. *Waste Manag.* **2000**, *20*, 561–568. [CrossRef]
138. Kritikaki, A.; Zaharaki, D.; Komnitsas, K. Valorization of Industrial Wastes for the Production of Glass–Ceramics. *Waste Biomass Valorization* **2016**, *7*, 885–898. [CrossRef]
139. Hao, J.; Dou, Z.-h.; Zhang, T.-a.; Wan, X.-y.; Wang, K. Energy conservation and emission reduction through utilization of latent heat of copper slag for iron and copper recovery. *J. Clean. Prod.* **2024**, *436*, 140602. [CrossRef]
140. Ye, C.L.; Zhang, M.J.; Yang, S.; Mweemba, S.; Huang, A.; Liu, X.; Zhang, X.L. Application of copper slags in encapsulating high-temperature phase change thermal storage particles. *Sol. Energy Mater. Sol. Cells* **2023**, *254*, 112257. [CrossRef]
141. Liu, J.; Su, Z.; Xu, J.; Zhang, Y. Thermal storage performance of $NaNO_3$/cordierite-mullite ceramic (CMC) composites deriving from metallurgical slag. *Ceram. Int.* **2023**, *49*, 38094–38102. [CrossRef]
142. Leng, G.; Qiao, G.; Jiang, Z.; Xu, G.; Qin, Y.; Chang, C.; Ding, Y. Micro encapsulated & form-stable phase change materials for high temperature thermal energy storage. *Appl. Energy* **2018**, *217*, 212–220. [CrossRef]

143. Liu, J.; Su, Z.; Xu, J.; Zhang, Y. Novel value-add recycling route of industry solid waste for acting as supporting skeleton of $NaNO_3$ phase change materials (PCMs). *J. Environ. Chem. Eng.* **2024**, *12*, 112332. [CrossRef]
144. Francis, A.A. Conversion of blast furnace slag into new glass-ceramic material. *J. Eur. Ceram. Soc.* **2004**, *24*, 2819–2824. [CrossRef]
145. Pan, D.a.; Zhang, S.; Bao, H.; Guo, B.; Liu, B. A Method for Preparing Hedenbergite Glass Ceramics by Lead Slag. Patent CN104773958A, 24 November 2017.
146. Chinnam, R.K.; Francis, A.A.; Will, J.; Bernardo, E.; Boccaccini, A.R. Review. Functional glasses and glass-ceramics derived from iron rich waste and combination of industrial residues. *J. Non-Cryst. Solids* **2013**, *365*, 63–74. [CrossRef]
147. Karamanov, A.; Taglieri, G.; Pelino, M. Sintering in nitrogen atmosphere of iron-rich glass-ceramics. *J. Am. Ceram. Soc.* **2004**, *87*, 1354–1357. [CrossRef]
148. Carlini, R.; Alfieri, I.; Zanicchi, G.; Soggia, F.; Gombia, E.; Lorenzi, A. Synthesis and Characterization of Iron-Rich Glass Ceramic Materials: A Model for Steel Industry Waste Reuse. *J. Mater. Sci. Technol.* **2016**, *32*, 1105–1110. [CrossRef]
149. Naimi, K.M.A.; Delclos, T.; Calvet, N. Industrial Waste Produced in the UAE, Valuable High-temperature Materials for Thermal Energy Storage Applications. *Energy Procedia* **2015**, *75*, 2087–2092. [CrossRef]
150. Koçak, B.; Fernández, A.I.; Paksoy, H. Characterization of demolition waste powder to be processed as sensible thermal energy storage material. *Sol. Energy Mater. Sol. Cells* **2021**, *230*, 111283. [CrossRef]
151. Agalit, H.; Zari, N.; Maaroufi, M. Suitability of industrial wastes for application as high temperature thermal energy storage (TES) materials in solar tower power plants—A comprehensive review. *Sol. Energy* **2020**, *208*, 1151–1165. [CrossRef]
152. Py, X.; Calvet, N.; Olives, R.; Meffre, A.; Echegut, P.; Bessada, C.; Veron, E.; Ory, S. Recycled Material for Sensible Heat Based Thermal Energy Storage to be Used in Concentrated Solar Thermal Power Plants. *J. Sol. Energy Eng.* **2011**, *133*, 031008. [CrossRef]

Disclaimer/Publisher's Note: The statements, opinions and data contained in all publications are solely those of the individual author(s) and contributor(s) and not of MDPI and/or the editor(s). MDPI and/or the editor(s) disclaim responsibility for any injury to people or property resulting from any ideas, methods, instructions or products referred to in the content.